https://doi.org/10.3311/PPci.22830

Periodica Polytechnica Civil Engineering

Mechanically Stabilized Earth Wall Reliability Analysis Using Response Surface Methodology, *ANN*, *ANFIS* and Multi-objective Genetic Algorithm

Nasser Sekfali[1*], Brahim Lafifi[2]

[1] Department of Architecture, Faculty of Earth Science, Badji Mokhtar University, P. O. B. 12, 23000 Annaba, Algeria
[2] Laboratory of Civil Engineering and Hydraulics, Faculty of Science and Technology, Université 8 Mai 1945, P. O. B. 401, 24000 Guelma, Algeria
[*] Corresponding author, e-mail: nasser.sekfali@univ-annaba.dz

Received: 19 June 2023, Accepted: 23 September 2024, Published online: 14 October 2024

Abstract

Considering uncertainty in the analysis of geotechnical structures is a necessary condition for optimal and robust design. An alternative method for studying the reliability of a mechanically reinforced earth wall in granular soil is used to account for these uncertainties more rigorously. This allows for the inclusion of various uncertainties in a mathematical risk formulation based on random variables. The deterministic model is a benchmark taken from the literature used in a numerical simulation to determine the maximum horizontal displacement of the wall. In this case, the serviceability limit state is considered, allowing the wall's actual behavior to be described. *ANOVA* was used to identify the most influential parameters on the system's response. As uncorrelated random variables, only the parameters (E, φ and γ) were considered. The mathematical model serving as the limit state function was numerically predictedby three methods, response surface methodology (*RSM*), artificial neural network (*ANN*) and Adaptive Neuro-Fuzzy Inference System (*ANFIS*), and their predictive capacities were then compared. The results showed that the *ANN* model outperformed the *RSM* and *ANFIS* models regarding prediction. *ANN* models and multi-objective genetic algorithm (*MOGA*) are used to optimize the Hasofer-Lind reliability index. The analysis is then carried out by taking into account the various types of functions of parameter distributions, which allowed us to better appreciate the effects of the uncertainties and identify the set of parameters with a high incidence.

Keywords

mechanically stabilized earth (MSE) walls, numerical modeling, reliability analysis, RSM, ANN, ANFIS, genetic algorithm

1 Introduction

Traditionally, the behavior of reinforced soil walls has been studied using deterministic methodologies that account for geotechnical parameter uncertainties using a global safety factor. The probability theory is used to more accurately account for uncertainty. We can account for the uncertainty associated with each parameter by using its probability distribution. Furthermore, these methods have the advantage of responding to the system (safety factor, maximum displacement) not only by its mean but also by its mean and standard deviation, reliability index, or probability of failure. As a result, reliability approaches enable considering the propagation of uncertainty related to the input parameters and the resulting system response by utilizing a mechanical model of the system under study.

Given the significant importance of reinforced soil structures, various numerical techniques,such as finite element (*FE*) and finite difference (*FD*), have been used for their performance-based design [1]. The variability of the geomechanical properties of soils justifies the reliability analysis of retaining walls. Recent studies of reinforced retaining walls have considered variations in reinforcing properties [2]. Yu and Bathurst [3] studied the engineering design optimization and the application of Monte Carlo simulation to evaluate the Hasofer–Lind reliability index. Several studies have been conducted on the lateral wall deformation of reinforced retaining walls.

The response surface methodology (*RSM*) has recently been used successfully in many fields of civil engineering. It simulates material behavior, structural problem optimization, experimental estimation, and concrete mix proportions. Karakayali et al. [4] used a probabilistic analysis of embankments to integrate the finite element, limit

Cite this article as: Sekfali, N., Lafifi, B. "Mechanically Stabilized Earth Wall Reliability Analysis Using Response Surface Methodology, *ANN*, *ANFIS* and Multi-objective Genetic Algorithm", Periodica Polytechnica Civil Engineering, 2024. https://doi.org/10.3311/PPci.22830

equilibrium, and *RSM*. Ghorbani and Sharifzadeh [5] applied the *RSM* to evaluate the Hasofer Lind reliability index in the case of a probabilistic analysis of a circular tunnel. Cepuritis [6] used *RSM* and the Second-order Reliability Method (*SORM*) to conduct a probabilistic investigation of rock excavation, taking the quadratic polynomial and cross terms into account to evaluate the limit state function. Hamrouni et al. [7] applied the *GA* to optimize the *RSM* for several geotechnical projects. Lafifi and Rouaiguia [8] investigated the reliability analysis of a shallow foundation using a combination of *RSM* and *MOGA*.

The *ANN* method has also been very successful in geotechnical engineering problems. *ANNs* were first applied in the early 1990s [9]. Khan et al. [10] used this tool to predict the residual strength of clay using data from the literature and a new prediction model, functional networks (*FNs*). Jahed Armaghani et al. [11] used 132 data sets to investigate the *ANN* in conjunction with the *PSO* algorithm to model the bearing load of socketed piles. Cheng et al. [12] proposed a new *ANN*-based *RSM* for predicting the failure probability of structures in conjunction with the uniform design method. In the case of a probabilistic slope stability analysis, Shu and Gong [13] integrated an *ANN*-based response surface to approximate the limit state function. Haeri et al. [14] investigated using a relatively simple nonparametric regression algorithm, multivariate adaptive regression splines (*MARS*), as an alternative to neural networks to approximate the relationship between pile strength and pile hammer impact stresses. Zhang et al. [15] proposed using a neural network (*NN*) tool to implement Monte Carlo Simulation (*MCS*) to overcome time-consuming numerical analysis for evaluating the impact of tunnel construction in a complex karst environment. Li and Yang [16] presented an *ANN* combined with *RSM* to demonstrate the probabilistic performance of geosynthetic reinforced soil.

The *ANFIS* approach has been used to predict the performance and stability of soil and rock formations, foundations, and other geotechnical structures in various geotechnical reliability studies. *ANFIS* was used by [17] to predict the bearing capacity of shallow foundations on cohesionless soils. The study created a model that considered soil parameters like relative density and angle of internal friction. Xue and Yang [18] used *ANFIS* to predict soil liquefaction potential during earthquakes. The study created a model considering a large database of liquefaction case histories. Harandizadeh et al. [19] used improved *ANFIS* to predict the bearing capacity of pile foundations in clay. The study developed a model that forecasted bearing capacity by considering information about different properties of soils and driven piles obtained from CPTs results.

This study presents a probability analysis of a mechanically stabilized earth wall reinforced by geosynthetics using the first-order reliability method to evaluate the Hasofer-Lind reliability index β_{HL} and the probability of failure (*FORM*). The deterministic model of the problem is generated by a two-dimensional numerical model created with the commercial software Plaxis [20], the treated problem's random variables are the geotechnical parameters of the soil, and the output response is the maximum horizontal displacement of the wall, denoted as $U_{h\max}$. A statistical tool based on the Analysis of Variance (*ANOVA*) was used to define the parameters influencing the maximum horizontal displacement of the wall used in the study to reduce the computational time required to generate the finite element models. *RSM*, *ANN* and *ANFIS* techniques were then used to predict the mathematical models relating to output responses and retained random variables. A comparison of these regression models is also carried out. Finally, the reliability index and failure probability are optimized using *ANN* models and the *MOGA*. This study also includes evaluating the design points and partial safety factors. Section 2 provides a detailed illustration of the adopted methodology.

2 Probabilistic approach

The probabilistic approach explicitly considers the uncertainties in strength and loads. The probability that the load exceeds the strength is expressed as

$$P[S > R] = P[R - S \le 0] = P[Z(x) \le 0], \tag{1}$$

where $\boldsymbol{X} = [x_1, x_2, \ldots, x_n]$ is the set of random variables, and $Z(x)$ represents the limit state function or performance function, with:

- $Z(x) = 0$ Limit state (boundary)
- $Z(x) > 0$ Let be the domain of safety
- $Z(x) < 0$ Let be the domain of failure.

Reliability, therefore, amounts to the direct integration of the joint density function expressed by

$$P_f = \int_{Z(x)<0} f(x)dx. \tag{2}$$

Where, $f(x)$ represents $\boldsymbol{X}$'s joint probability density function.

In practice, random variables are not explicitly mentioned in the limit state function, and the joint probability density function becomes unattainable for many random variables. Most of the time, we must settle for marginal laws relating to each random variable ***X***. As a result, depending on the correlation of variables and the complexity of integration, this integral can rarely be studied analytically or even numerically. Various resolution methods have been developed to overcome these difficulties [21].

2.1 First-Order Reliability Method (*FORM*)

The probability of failure P_f or the reliability index β, defined by Hasofer and Lind [22] in 1974, is used to assess a structure's safety by considering these uncertainties from a probabilistic standpoint. The authors generalized the approach and provided an exact and invariant definition for the reliability index. Its matrix formulation is as follows [21]:

$$\beta_{HL} = \min_{G(X)=0} \sqrt{(x-\mu)^T C^{-1} (x-\mu)} \,. \tag{3}$$

Where, ***X*** is the vector of n random variables, ***μ*** is the vector of mean values, and ***C*** is the covariance matrix.

The concept of reliability requires the construction of a failure scenario, which is defined using a so-called performance (or limit state) function, denoted $G(X) = 0$ and which separates the n-dimensional domain of random variables into two regions: a failure region represented by $G(X) \leq 0$ and a safety region given by $G(X) \geq 0$. The first step transforms the vector of physical random variables ***X*** into a reduced and independent centered normal space ***U*** (with zero means and unit standard deviation). This so-called iso-probabilistic transformation preserves the linearity of the limit state. The hyper-surface defined by $G(X) = 0$ can be expressed in the new space by $Z(U) = 0$. These variables are thus reduced by

$$u_i = \frac{x_i - \mu_{x_i}}{\sigma_{x_i}} \,. \tag{4}$$

The calculation of the reliability index, therefore, comes down to solving, in the normed space, the problem of optimization of Eq. (3) under constraints $Z(U) \leq 0$. This index can be interpreted geometrically by the minimum distance that separates the limit state from the origin in normed space. Thus, it is invariant in different representations of the same limit state. This definition was confirmed by [23] as the distance between the origin of the normed space and P^*, the most likelypoint of failure located on the limit state surface (Fig. 1).

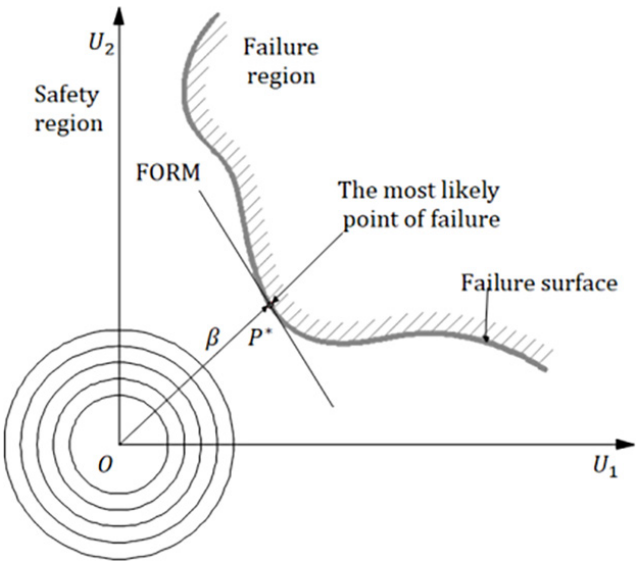

Fig. 1 FORM approximation for two random variables in standard space

A transformation to an equivalent normal distribution is required to apply the Hasofer-Lind method to random variables ***X*** with non-normal distributions. In the reduced space, the means and standard deviations are denoted by $\mu_{x_i}^N$ and $\sigma_{x_i}^N$ can be estimated by imposing two conditions [24]. At the design point on the failure surface, the distribution function and probability density of the non-normal variables should equal their equivalent normal value. The following relationships evaluate the standard deviation and mean of the equivalent normal distributions [25]:

$$\sigma_{x_i}^N = \frac{\varphi\left\{\varnothing^{-1}\left[F_i\left(x_i^*\right)\right]\right\}}{f_i\left(x_i^*\right)} \tag{5}$$

$$\mu_{x_i}^N = x_i^* - \varnothing^{-1}\left[F_i\left(x_i^*\right)\right]\sigma_{x_i}^N \,, \tag{6}$$

where φ is the probability density function of a normal variable, F_i is the cumulative function of non-normal distribution, f_i is the non-normal probability density function, and $\varnothing^{-1}[.]$ is the inverse of the cumulative function of the distribution of normal variables.

After determining $\sigma_{x_i}^N$ and $\mu_{x_i}^N$ for each variable, the relationship can express β more explicitly:

$$\beta_{HL} = \min_{G(X)=0} \sqrt{\left[\frac{x_i - \mu_{x_i}^N}{\sigma_{x_i}^N}\right]^T [R]^{-1} \left[\frac{x_i - \mu_{x_i}^N}{\sigma_{x_i}^N}\right]} \,, \tag{7}$$

where $[\boldsymbol{R}]^{-1}$ is the inverse of the correlation matrix.

Knowing the reliability index informs us about the level of security and also allows us to calculate the probability of failure P_f more or less precisely:

$$P_f \approx \varnothing(-\beta), \tag{8}$$

where $\varnothing$ is the normal cumulative distribution function.

Chen and Lind [26] proposed several optimization methods. One of the most well-knownsearch algorithms is that of [22]. These enhanced version algorithms are techniques that can be used in geotechnics.

3 Modeling methods

3.1 *RSM* approach

The technique of *RSM* is used as a practical predicting method to establish the relationship between various process parameters and responses. The goal is to investigate the relationship between these parameters and responses before optimizing the responses [27]. *RSM* aims to approximate the output response using an explicit function of the input parameters. This estimateis expressed as follows:

$$g(x) = a_0 + \sum_{i=1}^{n} a_i \times x_i + \sum_{i=1}^{n} a_i b_j \times x_i x_j + \sum_{i=1}^{n} b_i x_i^2 . \tag{9}$$

Where, x_i represents the input variables, n is the number of input factors and a_i, b_i, $a_i b_j$ are coefficients to be evaluated.

ANOVA is also useful for determining the factors that influence the response most. Computed coefficients of determination R^2 and adjusted R^2 provide information on the adjusted model's accuracy.

3.2 *ANN* approach

The *ANN* technique is a computational tool inspired by human brain neuron performance that can establish a mathematical relationship between input data and the output result of a defined problem [28]. Because of its exceptional capability, this technique has been used to solve complex problems. It has been suggested that in the case of evaluating complicated functions, these types of tools be used to approximate response functions. *ANN* is more robust and accurate than non-linear fitting, resolved with polynomial regression models [29]. The main factors that a user of this method must consider to achieve meaningful results are network type, architecture, and training parameters [28]. The network was designed by incrementally increasing the number of hidden layers and nodes until a suitable architecture was found.

According to [30], the hyperbolic tangent function is used in the neural network's hidden layers; this function speeds up network training compared to the sigmoid function [31]. Much of the data is set aside during the calculation for network training, while the remainderis used for validation. The backpropagation algorithm uses the descending gradient rule to train the network. This algorithm is based on minimizing the mean square error (*MSE*) by sequentially introducing input-output patterns to update weights each time. Minimizationis accomplished by shifting weights from the output to the input layer [30]. The first step in creating an *ANN* model is to choose an architecture network. The goal is to build a predicted *ANN* model while minimizing model size and errors during learning and validation [32]. In all of our cases, we used a learning rate of 0.01. To determine the optimal number of neurons in the hidden layer, we varied the number of iterations until we obtained a good R^2 and *RMSE*.

3.3 *ANFIS* approach

ANFIS is an artificial neural network that combines the capabilities of fuzzy logic and neural networks to perform adaptive modeling and intelligent decision-making. It is a powerful approach widely used in engineering, finance, medicine, and robotics. The method employs a fuzzy inference system (*FIS*), which employs fuzzy logic principles to improve human reasoning in uncertain and imprecise situations. Each variable in the *FIS* is treated as a linguistic variable expressed by various linguistic labels, and each label is assigned a membership function to measure the variable's degree of membership [33]. The *FIS* comprises if-then rules, with the premise and consequent parts defined by membership functions. *ANFIS* differs from traditional *FIS* by employing a hybrid-learning algorithm to incorporate human knowledge or specific data patterns into the rule base by adjusting the membership functions. *ANFIS* is based on the Takagi-Sugeno type, which does not use fuzzy sets in the consequent part but instead takes the form of if x is A, then $f = px + q$, where f is a linear combination of input variables with consequent parameters p and q. It is possible to simplify the fuzzy rule by reducing the first-order function to the constant term, where p equals 0 [34]. The *ANFIS* architecture is created by embedding the *FIS* into the adaptive network configuration; it has several advantages, including increased accuracy, interpretability, and flexibility, making it a valuable tool for modeling and prediction in various applications.

3.4 Performance parameters

Five commonly used measures were employed to assess the effectiveness of prediction models: coefficient of determination (R^2), mean square error (*MSE*), mean absolute percentage error (*MAPE*), root mean square error (*RMSE*),

and mean absolute deviation (*MAD*) [35]. These performance parameters were used to assess the models' performance from multiple angles, including the relationship between actual and predicted values, associated errors, and relative errors compared to actual or experimental values. The measures are expressed in Eqs. (10)–(14).

$$R^2 = \frac{\sum_{i=1}^{n}\left(y_{i,p} - y_{i,e}\right)}{\sum_{i=1}^{n}\left(y_{i,e} - y_{\text{average}}\right)^2} \tag{10}$$

$$MSE = \frac{\sum_{i=1}^{n}\left(y_{i,e} - y_{i,p}\right)^2}{n} \tag{11}$$

$$MAPE(\%) = \frac{100}{n}\sum_{i=1}^{n}\left|\frac{\left(y_{i,e} - y_{i,p}\right)}{y_{i,e}}\right| \tag{12}$$

$$RMSE = \frac{\sqrt{\sum_{i=1}^{n}\left(y_{i,e} - y_{i,p}\right)}}{n} \tag{13}$$

$$MAD = \frac{\sum_{i=1}^{n}\left|\left(y_{i,e} - y_{i,p}\right)\right|}{n} \tag{14}$$

Where, n is the number of the experiment, $y_{i,e}$, $y_{i,p}$ represent the experimental and the predicted values of the i^{th} experiment respectively, y_{average} is the average value of experimental data.

4 Numerical model

A reinforced earth wall was numerically modeled using the Plaxis 2D finite element calculation code [20]. The numerical model chosen is a benchmark proposed by [7]. It represents a 6 m high wall made up of four superimposed panels (modeled by elements plate) and reinforced by eight levels of geosynthetic reinforcements (modeled by geogrid elements) of four meters in length (Fig. 2).

The panels (Fig. 3) are modeled by 1.5 m square plates. Table 1 shows their limit resistances in tension and compression. The shape of these prospects a complex three-dimensional geometry of the wall facade. A two-dimensional model with continuous reinforcements can be used to simplify this geometry. The calculation width is then reduced to two panels to simplify things further (4 reinforcement strips for each panel).

The reinforcement parameters are calculated by homogenizing the geometric properties for the width under consideration. The model comprises two soils (Fig. 2), the

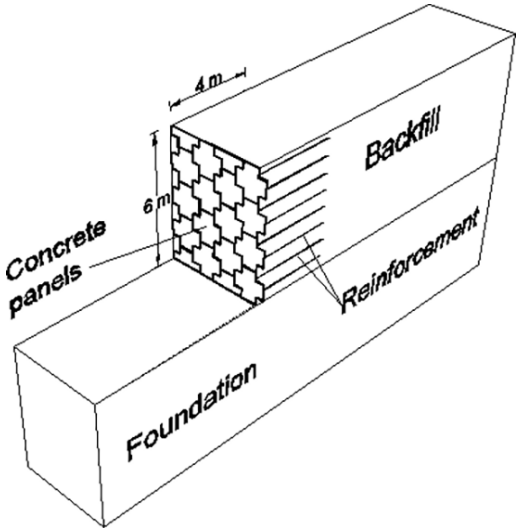

Fig. 2 The numerical model

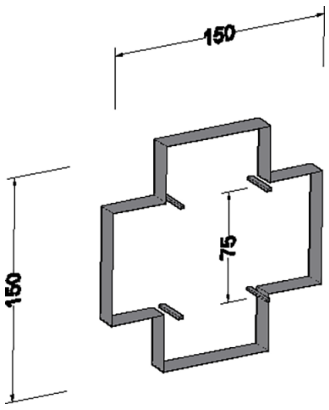

Fig. 3 Concrete panels

characteristics of whichare shown in Table 1. The reinforced backfill is simulated by a uniform fine sand known as Hostun RF sand [36]. The reinforced embankment behavior model is a linear elastic and perfectly plastic model with a Mohr-Coulomb-type failure criterion, and the mechanical parameters are obtained through calibration on triaxial tests [37]. A linear elastic behavior model is used for the foundation soil. The horizontal and vertical displacements are blocked at the model's base for the boundary conditions, but only the horizontal displacements are blocked on the lateral sides.

The reinforcements simulated in the reference calculation correspond to GeoStrap 50 (*GS 50*) geosynthetic reinforcements currently used in Reinforced Earth walls. Table 1 summarizes the properties considered in the model. The extensible reinforcements of type (*GS 50*) are typically implemented as a pair of 50 mm wide strips (250 mm) in most real walls. Their modeling in Plaxis software [20] using structural elements of the "Geogrids" type allows them to consider tension, compression, and shear

Table 1 Mechanical properties of soils, concrete and reinforcement [7]

Properties (unity)	Fill	Soil foundation	Concrete panels	Reinforcement *GS 50*
E (Young's modulus) (MPa)	50	50	15000	2500
v (Poisson ratio)	0.3	0.3	0.2	-
φ (friction angle) (°)	36	-	-	-
Ψ (dilatation angle) (°)	6	-	-	-
C (cohesion) (KPa)	0	-	-	-
Unit weight (kN/m^3)	15.6	20	25	-
Width (m)	-	-	-	0.1
Thickness (mm)	-	-	-	3
Strip tensile yield-force limit (kN)	-	-	-	100
Maximum compressive strength (kPa)	-	-	-	0
Tensile failure strain limit of the strip (%)	-	-	-	12

resistance. To achieve more realistic modeling, the reinforced backfill must be placed in 0.375 m layers throughout all construction phases:

- Stage 1: Installation of the first concrete panel, the first and second layers, and the first reinforcement between the two reinforced backfill layers (equilibrium under self-weight).
- Stage 2: The third and fourth layers and the second reinforcement between the two layers of reinforced backfill (equilibrium under self-weight) are installed.
- Stage 3: Installation of the second concrete panel, the fifth and sixth layers of backfill, and the third reinforcement (equilibrium under self-weight).

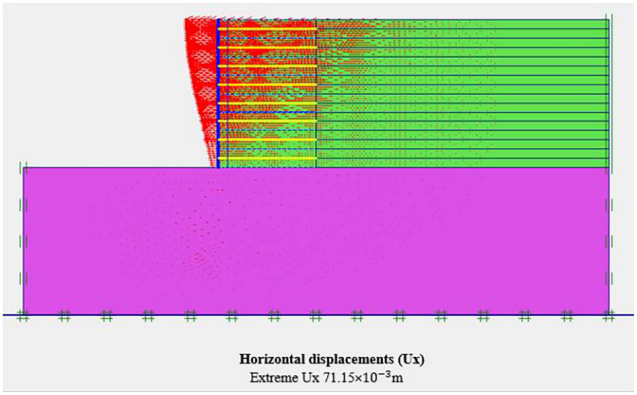

Fig. 4 Horizontal displacements (m) in the reinforced earth wall with Plaxis 2D

These phases were repeated until the wall's height (6 meters) was reached. The calculations were performed in drained conditions, and the water table's presence was not considered. The friction angle at the interface is assumed to be two-thirds of the friction angle in the soil.

4.1 Experimental design

The numerical model will perform numerous deterministic calculations assuming all input variables are random. The probabilistic technique becomes extremely time-consuming to compute as the number of random variables increases [7]. To address this issue, *ANOVA* analyzed the design of the experiment to determine which input parameter had the greatest influence on the wall behavior and to reduce computation time.

In our study case, the maximum horizontal displacement U_{hmax} was taken into account (Fig. 4). Experiment design is a useful tool for reducing operation time. As a result, the design of experiments can be used to reduce costs during the design process. A full factorial design and *ANOVA* are typically used to assess the impact of many input factors on the overall behavior of the output results. Several random input parameter values are chosen and varied within the context of the factorial design. Each combination is numerically simulated, and the results are saved [38]. For each random input parameter, n values were chosen, yielding a total of n^k combinations for the k point to be numerically simulated.

When the number of input parameters is small, the full factorial design generates a reasonable number of combinations. However, as their number grows, simulations based on this design become more computationally difficult. As a result, only a subset of the total n^k factorial design combinations must be investigated because higher-level interactions between the input factors are frequently irrelevant, and the focus is on the major effect of each parameter. The n^k simulations to realize can be replaced with only $2^{(k-p)}$ combinations, where 2^p is the number of simulations deduced from the initial factorial design [38].

This research aims to identify the most important random variables that influence the behavior of the wall. Only half of the experimental design was used with $p = 1$. As a result, the full factorial design (n^k) will be replaced by a fractional design with $n^{(k-1)}$ configurations, where k represents the number of random variables, and n is the level number of each parameter.

4.2 Fractional design (Central Composite Design)

The central composite design is a well-known technique for optimizing with a quadratic regression model (*CCD*). Each variable in this methodcan have five levels, with two of those levels representing the same extreme two factorial points as in the full factorial design. While each factor's mean value represents its third level, the last two levels are considered axial points and are represented by an axial distance called often (alpha), which is added to or subtracted from the mean value of each variable.

The *CCD* technique provides efficient designs for problems with fewer than four parameters, and the number of consecutive runs iscomparable.In the current study, a design of experiments (*CCD*) with three levels and five factors was used to assess the effect of random input variables on wall behavior. In our case, the output results are the maximum horizontal displacement $U_{h\max}$ of the wall, while the five random factors are: Young's modulus (E), Poisson coefficient (v), the friction angle (φ), unit weight (γ) and the dilatancy angle (Ψ). Their levels are listed in Table 2.

A total of 27 experiments were carried out using the validated numerical model, according to a central composite design with 5 factors and 3 levels. The total realization was calculated using the formula $2^{n-1} + 2n + m$, where n is the number of random variables, and m is the number of replicated points. As a result, we obtained 16 factorial points, 10 axial points, and one replicated center point, with $\alpha = 1$. The obtained results of the random numerical models are listed in the last column of Table 3, followed by *ANOVA* to evaluate the influence of each random variable on the response. Only parameters with a contribution greater than 5% were kept for the remainder of the study.

Table 2 Levels of soil parameters used in the numerical models

Input parameters	Minimal value of μ	Mean value of μ	Maximal value of μ
Unit weight (kN/m^3)	13.0	17.5	22.0
E (Young's modulus) (MPa)	30.0	60.0	90.0
v (Poisson ratio)	0.2	0.3	0.4
φ (friction angle) (°)	25.0	32.5	40.0
Ψ (dilatation angle) (°)	0.0	7.0	14.0

4.3 *ANOVA* results

The Analysis of Variance (*ANOVA*) is a statistical method for interpreting the results. It categorizes the various input parameters based on their impact on the output parameters. Table 3 shows the *ANOVA* results with a significance level of $\alpha = 0.05$ (i.e., for a 95% reliability level). A low probability value (≤ 0.05) indicates that the models obtained are statistically significant. Table 4 shows that the friction angle has the greatest influence on the response, with a contribution of 40.821%, followed by the unit weight gamma, with a contribution of 12.877%, and Young's modulus E, with a contribution of 6.564%. While the terms Ψ and v had the least influence, contributing 1.899 and 1.584%, respectively. Except for the terms ($v \times \Psi$) and ($\varphi \times \Psi$), which indicate a contribution greater than 5.0%, the rest of the interaction terms were found to be negligible. Based on the *ANOVA* results, we used friction angle, unit weight, and Young's modulus as random variables in the remainder of the study.

4.4 Methodology

Three random variables were considered based on *ANOVA*. They are characterized by their mean values μ_i and their coefficients of variation Cov_i. We evaluated the performance function $g(x)$ at the mean value point and the $2n$ points, each at $\pm k$ where $k = 1.65$ (Table 5). Single replicate 3^n factorial design was used to fit a quadratic regression model, where n is the total number of input variables. Throughout the rest of the study, a full factorials design of experiments (L27) was used, corresponding to 27 sample points for three input variables (E, φ and γ), where the output response, which depends on the random variables, is the performance function (G). The investigation aimed to assess the impact of controllable factors on output response.

In a more general framework, the literature provides an overview of the dispersion and the choice of the type of distribution of the probability density of these parameters for the selection of the variation range of the design parameters of our problem. According to Wolff [39], the probability density of the internal friction angle (φ) in sands is normally distributed. Griffiths et al. [40] used a Lognormal distribution for the unit weight (γ) and the internal friction angle (φ) with the coefficients of the following variations

Table 3 Levels of soil parameters used in the numerical models

Run	Young's modulus E (MPa)	Poisson coefficient v	Unit weight γ (kg/m^3)	Friction angle φ (°)	Dilatancy angle Ψ (°)	Horizontal displacement $U_{h\max}$ (cm)
1	60	0.3	13	32.5	7	3.6
2	30	0.2	22	25	0	9.26
3	90	0.2	22	40	0	1.19
4	90	0.2	13	40	14	3.42
5	30	0.3	17.5	32.5	7	5.42
6	30	0.4	22	40	0	5.39
7	60	0.3	17.5	32.5	14	3.87
8	90	0.4	22	40	14	2.71
9	90	0.4	13	25	14	4.76
10	90	0.2	13	25	0	1.43
11	30	0.4	22	25	14	5.96
12	30	0.2	13	25	14	5.91
13	30	0.2	22	40	14	5.21
14	30	0.4	13	25	0	8.09
15	60	0.2	17.5	32.5	7	4.66
16	60	0.3	22	32.5	7	5.65
17	90	0.2	22	25	14	5.98
18	60	0.4	17.5	32.5	7	4.56
19	60	0.3	17.5	25	7	8.21
20	60	0.3	17.5	32.5	7	4.62
21	60	0.3	17.5	32.5	0	5.63
22	30	0.4	13	40	14	2.63
23	90	0.3	17.5	32.5	7	4.18
24	60	0.3	17.5	40	7	1.97
25	90	0.4	13	40	0	0.76
26	90	0.4	22	25	0	12.78
27	30	0.2	13	40	0	3.58

to demonstrate the strong effect of failure mechanisms in spatially random materials: Cov_γ = 50% Cov_φ = 17.32%. Sivakumar Babu and Srivastava [41] confirmed the interest in the application of the surface method (*RSM*) in a probabilistic analysis by adopting in their cases a normal distribution for the parameters (φ, γ and E) and a coefficient of variation, respectively, as follows: Cov_φ = 6%, Cov_γ = 6% and Cov_E = 12%.

Youssef Abdel Massih and Soubra [42] demonstrated that for a serviceability limit state, precisely evaluating the uncertainties of Young's modulus (E) was critical in obtaining reliable probabilistic results. The lognormal distribution was used, with a coefficient of variation of Cov_E = 15%. Based on these findings and those of [23], we calculated the design parameters by selecting different cases of combinations of the Normal and Lognormal distributions, with the corresponding coefficients of variation shown in Table 5. Uncorrelated variables were used in all of these cases to simplify things.

5 Results and discussion

Table 6 lists the results for the case of a maximum horizontal displacement $U_{h\max}$ = 10.0 cm, with the random variables represented by E, φ and γ. The performance function (G_{10}) illustrates the calculated and the estimated output resultsby *RSM*, *ANN* and *ANFIS* models, according to the L27 full factorial design.

5.1 *RSM* modeling

RSM is a combination of statistical and mathematical techniques that can be used to model and analyze a problem. It determines the best approximation for the true functional

Table 4 *ANOVA* results

Source	Sum of squares	df	Mean square	*F* value	*p*-value Prob > *F*	Cont.%	
Model	171.70	15	11.45	28.15	<0.0001		Significant
A - Young's modulus	11.27	1	11.27	27.71	0.0003	6.564	Significant
B - Poisson's coefficient	2.72	1	2.72	6.70	0.0252	1.584	Significant
C - Unit weight	22.11	1	22.11	54.39	<0.0001	12.877	Significant
D - Friction angle	70.09	1	70.09	172.40	<0.0001	40.821	Significant
E - Dilatancy angle	3.26	1	3.26	8.02	0.0163	1.899	Significant
A × *B*	7.40	1	7.40	18.20	0.0013	4.310	Significant
A × *C*	2.79	1	2.79	6.86	0.0239	1.625	Significant
A × *D*	1.24	1	1.24	3.06	0.1082	0.722	Significant
A × *E*	3.35	1	3.35	8.24	0.0152	1.951	Significant
B × *C*	0.68	1	0.68	1.67	0.2222	0.396	Significant
B × *D*	7.45	1	7.45	18.33	0.0013	4.339	Significant
B × *E*	16.04	1	16.04	39.45	<0.0001	9.342	Significant
C × *D*	5.86	1	5.86	14.40	0.0030	3.413	Significant
C × *E*	8.44	1	8.44	20.76	0.0008	4.916	Significant
D × *E*	9.00	1	9.00	22.14	0.0006	5.242	Significant
Residual	4.47	11	0.41				
Cor total	176.17	26					

Table 5 Variation values of the random variables

Input parameters	Mean (μ)	Standard deviation (σ)	*Cov* (%)	$\mu - 1.65\sigma$	$\mu + 1.65\sigma$	Distribution
Friction angle φ (°)	36.0	3.6	10	30.06	41.94	Normal/Lognormal
Unit weight γ (kN/m^3)	15.60	1.248	8	13.54	17.66	Normal
Young's modulus E (kN/m^2)	50	7.5	15	37.63	62.38	Normal/Lognormal

relationship between the response and the set of independent variables [43], and polynomial functions commonly approximate it in cases where models are obtained by conducting a small number of experiments using the design of experiments. A quadratic regression model modeled the relationship between the inputs (Young's modulus E, friction angle φ and unit weight γ) and the output (performance function G_{10}) and presented by Eq. (15) with a coefficient of determination R^2 of 96.88% using Design Expert V10 Software [44].

$$\begin{aligned} G_{10} &= 63.017 - 0.083 \times E - 3.141 \times \varphi + 0.577 \times \gamma \\ &+0.00379 \times E \times \varphi - 0.0015 \times E \times \gamma + 0.029 \times \varphi \times \gamma \\ &-0.000139 \times E^2 + 0.0325 \times \varphi^2 - 0.0552 \times \gamma^2 \end{aligned} \quad (15)$$

This regression model approximates the response G_{10} based on the input design parameters (E, φ and γ).

5.1.1 Graphical validation of the model

Fig. 5 displays the normal probability diagram of the residual for the treated response. We examined the accuracy of the approximated model listed above for the best output response accuracy. It is worth noting that the condition of the residual normality plot is satisfied because their approximation is in the form of a straight line.

5.2 *ANN* modeling

Fig. 6 illustrates the adequate *ANN* architecture of the performance function G_{10} model (3-3-1) with three input nodes (E, φ and γ), three nodes in the hidden layer and one node for the output layer (the response G_{10}). This final architecture was obtained after an optimal number of 50 iterations.

The mathematical model for the *ANN* architecture is presented by Eq. (16). This model results from the product of hidden layers of the height neurons to a linear function.

$$G_{10} = 1.3785 \times H_1 - 0.9137 \times H_2 - 2.1845 \times H_3 + 5.7332 \quad (16)$$

Where, $H1$ to H3 are the outputs of each neuron of the hidden layer and are expressed as below:

Table 6 Results for the case of the performance function (G_{10})

Run	Factor 1	Factor 2	Factor 3	Response G_{10} (cm)			
	A: Young's modulus *E* (kPa)	*B*: Friction angle φ (°)	*C*: Unit weight γ (kN/m^3)	Calculated	*RSM*	*ANN*	*ANFIS*
1	37.63	36	17.66	5.13	5.24	5.11	5.13
2	50	41.94	15.6	5.49	5.39	5.48	5.52
3	37.63	41.94	15.6	7.52	7.17	7.41	7.52
4	50	30.06	17.66	4.75	4.55	4.75	4.75
5	62.38	36	17.66	4.61	4.75	4.66	4.74
6	50	30.06	13.54	5.09	4.98	5.10	5.09
7	62.38	41.94	17.66	4.05	4.23	4.17	4.49
8	37.63	30.06	13.54	6.00	6.14	6.02	6.00
9	37.63	36	13.54	4.56	4.81	4.60	4.56
10	50	36	15.6	5.11	5.21	5.12	5.12
11	37.63	30.06	17.66	7.32	7.12	7.39	7.32
12	50	36	17.66	7.44	7.56	7.45	7.45
13	62.38	41.94	15.6	4.89	5.03	4.88	5.16
14	50	30.06	15.6	7.38	7.64	7.45	7.38
15	62.38	36	15.6	4.46	4.41	4.46	4.53
16	62.38	36	13.54	5.67	6.01	5.66	5.70
17	37.63	30.06	15.6	5.11	4.93	5.18	5.11
18	62.38	30.06	15.6	5.13	5.05	5.13	5
19	62.38	30.06	17.66	5.51	5.70	5.49	5.54
20	62.38	30.06	13.54	6.35	6.25	6.34	6.46
21	37.63	41.94	13.54	5.35	5.19	5.35	5.17
22	37.63	41.94	17.66	7.43	7.62	7.45	7.51
23	62.38	41.94	13.54	5.5	5.40	5.49	5.54
24	50	41.94	17.66	4.64	4.52	4.64	4.62
25	37.63	36	15.6	4.61	4.51	4.67	4.66
26	50	41.94	13.54	5.49	5.54	5.50	5.48
27	50	36	13.54	7.43	7.02	7.37	7.32

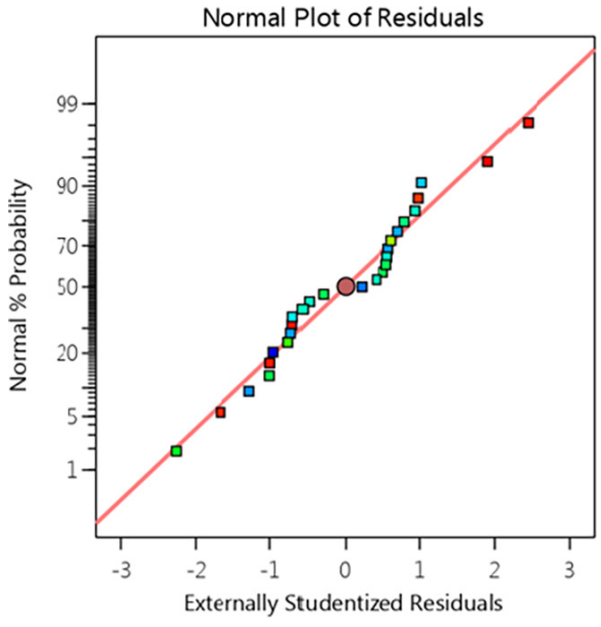

Fig. 5 Normal probability of residuals for the performance function G_{10}

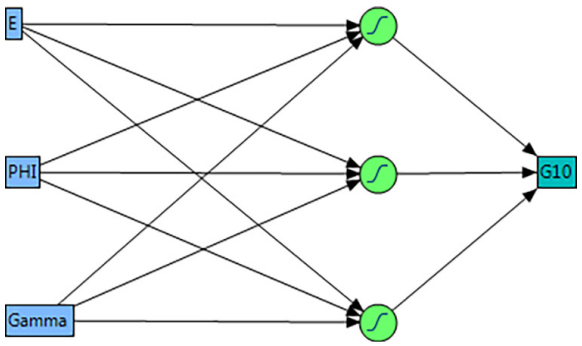

Fig. 6 *ANN* architecture (3-3-1) for the performance function G_{10}

$$\left.\begin{aligned} H_1 &= \tanh\left(0.5\times\begin{pmatrix}0.03286\times E+1.6679\times\varphi\\ -0.3017\times\gamma-56.3467\end{pmatrix}\right)\\ H_2 &= \tanh\left(-0.5\times\begin{pmatrix}0.082979\times E+0.84857\times\varphi\\ +0.01698\times\gamma-32.1219\end{pmatrix}\right)\\ H_3 &= \tanh\left(0.5\times\begin{pmatrix}0.0288\times E+1.91177\times\varphi\\ +1.7397\times\gamma-90.34967\end{pmatrix}\right)\end{aligned}\right\}. \quad (17)$$

Fig. 7 illustrates the predicted and calculated results for training and validation cases.

Fig. 7 shows that the intersection between calculated and predicted values of the response G_{10} is close to the median line. Moreover, the value of the coefficient of determination R^2 is 0.9989 for the training case and 0.9969 for the validation case, and the value of *RMES* is 0.0327 and 0.0641 for both cases, respectively. This finding highlights the robustness of the fitted mathematical model.

5.3 *ANFIS* modeling

In this study, an *ANFIS* model was proposed to predict the performance function G_{10} based on three input variables: E, φ and γ. The model used a first-order fuzzy inference system of the Sugeno method and had a five-layer architecture consisting of fuzzification, product, rule or normalization, defuzzification, and overall summation, and the Gaussian membership function was chosen. The architecture of the proposed model is illustrated in Fig. 8. Descriptions of these layers have been previously reported in previous works [45]. The data was divided into a training set (70%) and a validation set (30%) to test the generalization capacity of the model. The modeling and analysis were conducted using the fuzzy logic toolbox of MATLAB - MathWork Inc. (version R2015b) [46].

The last column of Table 6 presents the results of the *ANFIS* model's prediction of the performance function G_{10}. To evaluate the model's fitness, R^2 values were determined, resulting in values of 0.990 for training and 0.992 for the testing, respectively. An R^2 value of 0.990 indicates that the model can explain 99% of the variation between the actual and estimated values. Additionally, Fig. 9 displays the correspondence plot of the estimated G_{10} versus the actual G_{10}, indicating reasonable agreement between the estimated and actual performance function.

5.4 Comparison of *RSM*, *ANN* and *ANFIS* models

The *RSM*, *ANN* and *ANFIS* methods were compared to determine the predictive model's accuracy. Some comparisons were required in this step to demonstrate the difference between calculated results and predicted values obtained by *RSM*, *ANN* and *ANFIS* models (Fig. 10). The highest coefficient of determination is R^2, and low values of the mean square error (*MSE*), mean absolute percentage error (*MAPE*), root mean square error (*RMSE*), and mean absolute deviation (*MAD*). Fig. 10 shows the differences between calculated and predicted responses using *RSM*, *ANN* and *ANFIS* models. It is worth noting that the measured and *ANN*-predicted values are very close compared to the *RSM* and *ANFIS* predicted values. The *RSM* and *ANFIS* models yielded a coefficient R^2 of 0.968 and 0.990, respectively. The corresponding value

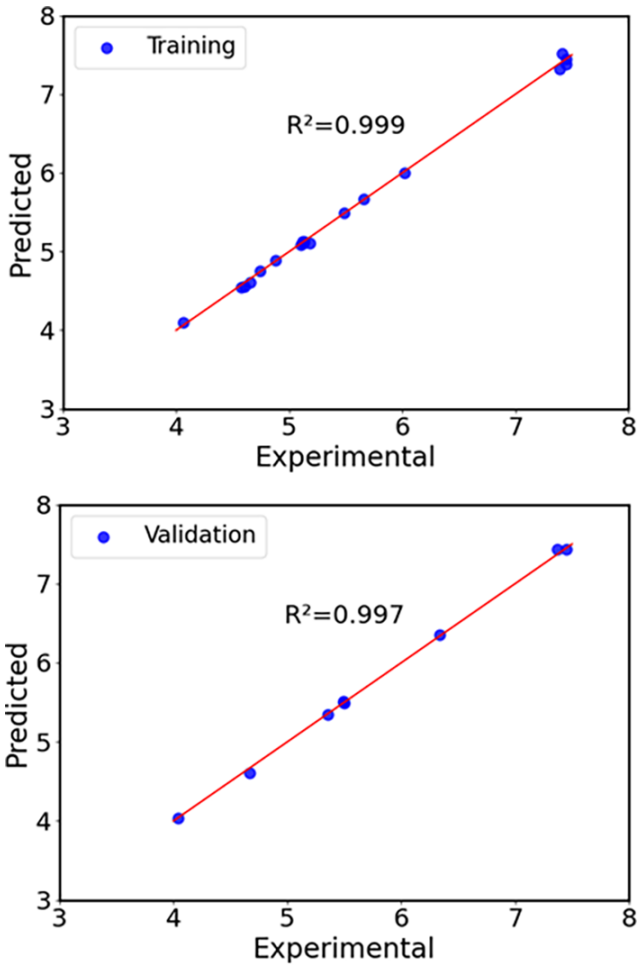

Fig. 7 *ANN* predicted versus calculated values for G_{10}

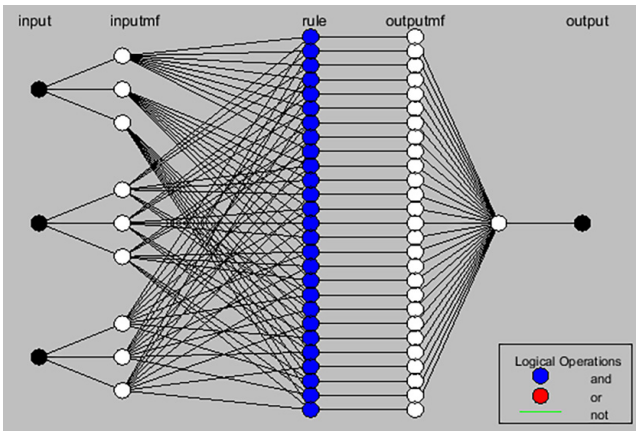

Fig. 8 *ANFIS* architecture for the performance function G_{10}

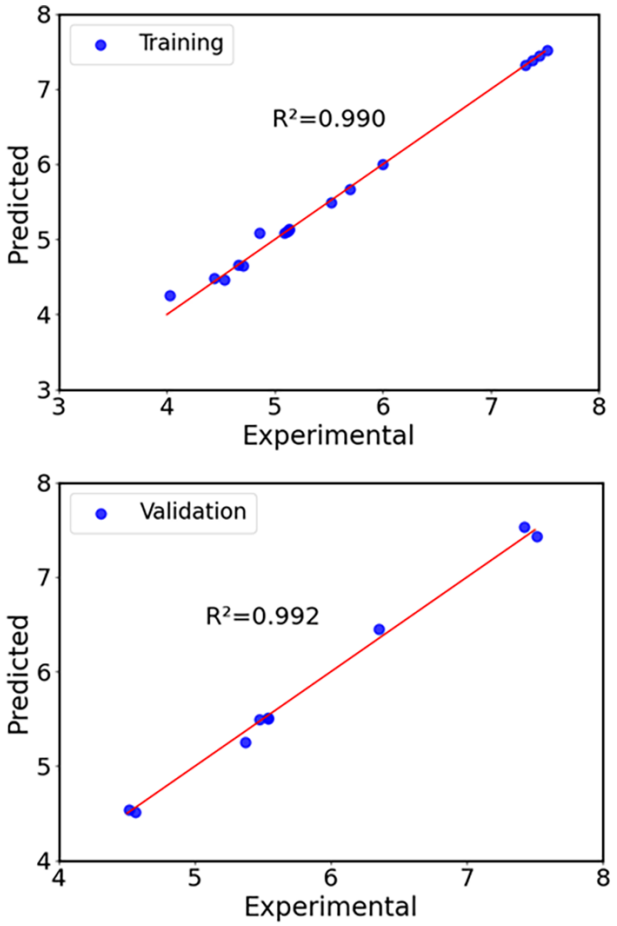

Fig. 9 *ANFIS* predicted versus calculated values for G_{10}

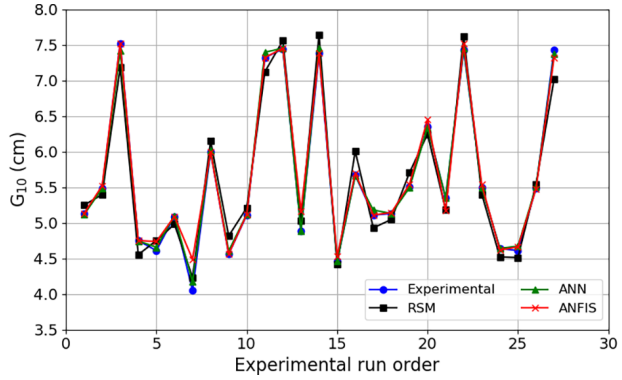

Fig. 10 Comparison between predicted and experimental values for G_{10} with *RSM*, *ANN* and *ANFIS* models

from the *ANN* model is 0.998 (Table 7). It can be noted that the *MSE*, *MAPE*, *MAD* and *RMSE* estimated values from the *ANN*-fitted model are more accurate than those from the *RSM* and *ANFIS* models (Table 7). As a result, *ANN* models were used for the optimization process.

6 Optimization using a *MOGA*

The multi-objective optimization aimsto find a compromise between several criteria and compute the input parameter values that can be brought to the optimal values of the response outputs while considering some criteria [47]. There are numerous optimization methods for solving both constrained and unconstrained problems. The most widely used optimization methods are genetic algorithms (*GAs*). Creating an arbitrarily initial population called chromosomes can be considered an initial solution whose main performance is evaluating the fitness function. The resultsare then used to generate potential solutions using evolutionary techniques such as selection, crossing, and mutation. The resolution system may repeat this procedure until the best solution is obtained [48].

Table 7 Comparison between *RSM*, *ANN* and *ANFIS* models

Index	R^2	*MSE*	*MAPE*	*MAD*	*RMSE*
RSM	0.968	0.0362	2.94	0.167	0.189
ANN	0.998	0.002	0.56	0.031	0.046
ANFIS	0.990	0.013	1.23	0.061	0.115

A combination of the minimization of the Hasofer-Lind reliability index β_{HL} and the cancellation of the performance function was carried out. The *MOGA* tool was employed based on the mathematical model formulated using the *ANN* method. The constraints used in the present optimization are:

$$\text{Minimise } \beta_{HL} = \sqrt{(X')^T C^{-1}(X')} \text{ with } G_{10}(x^*) = 0\,. \quad (18)$$

The limitations of the input factors for the performance functions models are given by Eq. (19):

$$\left.\begin{aligned} E_{\min} \le E \le E_{\max} \\ \varphi_{\min} \le \varphi \le \varphi_{\max} \\ \gamma_{\min} \le \gamma \le \gamma_{\max} \end{aligned}\right\}. \quad (19)$$

Matlab software [46] was used to create a program file containing the fitness functions. The fitness functions, in this case,are the Hasofer-Lind reliability index β_{HL} and the performance function *G*. The population, crossover distribution index, mutation distribution index, crossover probability, and mutation probability of the *MOGA* were all set using the *GA* toolbox in Matlab software [46]. Table 8 summarizes the β_{HL} results and the corresponding design points (E^*, φ^* and γ^*), for various horizontal displacement values $U_{h\max}$.

Table 8 outlines the reliability index results and the corresponding design points of the mechanical parameters (Density, internal friction angle, and modulus of elasticity) for various limit values of horizontal displacement (5 to 20 cm) and cases of distribution combinations. It can be noted that the reliability index directly depends on the limit displacements in these various cases. Increasing

Table 8 Reliability indices, design points and partial safety factors with the *ANN* models

$U_{h\max}$ (cm)	β_{HL}	P_f (%)	γ^* (kN/m^3)	φ^* (°)	E^* (kPa)	F_γ	F_φ	F_E
Case with Normal, Normal and Lognormal, respectively, for γ, φ and E								
5	0.881	18.920	15.798	39.120	49.581	1.013	0.893	1.008
10	1.470	7.080	16.042	31.430	44.588	1.028	1.189	1.121
15	3.386	0.035	16.526	24.543	42.815	1.059	1.591	1.168
20	5.512	0.177e-5	17.450	17.564	39.005	1.119	2.295	1.282
Case with Normal, Lognormal and Normal, respectively, for γ, φ and E								
5	0.791	21.450	15.766	38.349	47.499	1.011	0.918	1.053
10	1.462	7.190	16.081	31.358	45.008	1.031	1.192	1.111
15	3.366	0.038	16.562	24.517	43.188	1.062	1.593	1.158
20	5.581	0.119e-5	17.494	17.269	39.003	1.121	2.337	1.282
Case with Normal variables for γ, φ and E								
5	0.880	18.940	15.828	39.099	50.052	1.015	0.894	0.999
10	1.501	6.670	16.074	31.372	44.928	1.030	1.192	1.113
15	3.405	0.033	16.559	24.519	43.162	1.062	1.593	1.158
20	5.632	0.89e-6	17.493	17.198	39.003	1.121	2.347	1.282

the limit displacement leads to a constantly higher index. Similarly, a slight increase was observed when all variables had a normal distribution. The value of β_{HL} increases by 2.5% for the same limit displacement; this small difference can take on larger values if we consider non-normal distributions for all variables. This result is due to the fact that normal and non-normal distributions differ in the areas of different design points [7]. Therefore, using normal distributions prioritizes safety over other probabilistic models that may result in an uneconomic design. Furthermore, the partial safety factors are obtained by dividing the characteristic values by the calculation values "design point" (γ^*, φ^* and E^*) are expressed as follows:

$$F_\gamma = \frac{y^*}{\mu_y} \tag{20}$$

$$F_\varphi = \frac{\tan \mu_\varphi}{\tan \varphi^*} \tag{21}$$

$$F_E = \frac{\mu_E}{E^*} . \tag{22}$$

Where, μ_y, μ_φ and μ_E represent the mean value of the unit weight, the internal friction angle and the modulus of elasticity, respectively.

These factors are also directly dependent on the limit displacement in all cases, which can converge to the value 1 for the limit case of the horizontal displacement equal to (7.1 cm). Compared to the other parameters (φ and E), the partial safety factors for the unit weight (γ) present a fine sensitivity to the limit displacement. They always take values close to 1 in most cases. As a result, this variable has always been considered a deterministic parameter. Nottrodt [49] reached similar findings. On the other hand, for the low limit displacement (5 cm), the partial safety factors of φ and E are less than one, which is explained by the inverse effects of the parameters on the behavior of the model. The decrease in φ and E leads to an increase in γ. This result is in good agreement with the study of [7].

7 Conclusions

A probabilistic analysis is performed on a mechanically reinforced earth wall in granular soil. A numerical simulation was used as a deterministic model to evaluate the horizontal displacement of the wall face. The serviceability limit state is thought to accurately describe the wall's actual behavior. Following an *ANOVA* statistical analysis demonstrating the degree of influence of the various parameters on the displacement of the wall, only the parameters (γ, φ and E) are considered uncorrelated random variables. By comparing the three methods (*RSM*, *ANN* and *ANFIS*), the functional relationship between the input and output variables, representing the limit state, is obtained (*ANN*). In this case, the Hasofer-Lind index is used to evaluate the reliability index of the reinforced earth wall, which is accomplished through multi-objective optimization using a *GA*. This comparison allowed us to deduce the effects of design parameter uncertainties on the reliability index.

By calculating each parameter's percentage contribution, the statistical analysis *ANOVA*-type can identify the most influential parameters on the wall's behavior. It should be noted that any parameter with a contribution of more than 5% is considered a probabilistic variable. The usefulness of this method was justified by considering the low contribution of density, which results in a fine dependence on the limit displacement, resulting in partial safety factors close to 1 in most cases. Furthermore, its advantage over other research works is useful in developing good judgment and improving decision-making. Based on the data set,an objective comparison of the tree methods (*RSM*, *ANN* and *ANFIS*). Reveals that the predictive models developed by the (*ANN*) method are by far the most accurate and that the latter was very relevant for the objective, in contrast to that carried out using the statistical program (*RSM*) based on different types of mathematical methods, such as the complete quadratic, the pure quadratic, the interactions, and the linear regression.

In comparison to the size of the search space, the *GA* technique finds the global optimum in a relatively small number of evaluations. The *GA* is much less likely than point-to-point motion optimization techniques to converge to a local optimum. In contrast to traditional methods, which rely on the existence and continuity of derivatives, they use only objective information about the function or physical condition. The results confirmed previous parametric studies, indicating that the partial safety factors for unit weight always take values close to one in most cases. This is why this parameter has been referred to as a deterministic variable in previous works.

Furthermore, the partial safety factors of the parameters (φ and E) exhibit a remarkable dependence on the limit displacement (U_{max}), which explains their observed influences on the displacement of the wall, particularly that of the internal friction angle, which contributes significantly in this case. For small limit displacements less than 7.1 cm, the reliability index converges towards values less than one, indicating high failure probabilities and the vulnerability of the structure in question. Following the results of the various distribution combinations used, considering a normal distribution for all random variables appears sufficient, putting the situation on the safe side and leading to an uneconomical design.

References

[1] Skinner, G. D., Rowe, R. K. "Design and Behaviour of Geosynthetic-Reinforced Soil Walls Constructed on Yielding Foundations", Geosynthetics International, 10(6), pp. 200–214, 2003. https://doi.org/10.1680/gein.2003.10.6.200

[2] Sayed, S., Dodagoudar, G. R., Rajagopal, K. "Reliability Analysis of Reinforced Soil Walls Under Static and Seismic Forces", Geosynthetics International, 15(4), pp. 246–257, 2008. https://doi.org/10.1680/gein.2008.15.4.246

[3] Yu, Y., Bathurst, R. J. "Probabilistic Assessment of Reinforced Soil Wall Performance Using Response Surface Method", Geosynthetics International, 24(5), pp. 524–542, 2017. https://doi.org/10.1680/jgein.17.00019

[4] Karakayali, M. K., Foschini, G. J., Valenzuela, R. A. "Network coordination for spectrally efficient communications in cellular systems", IEEE Wireless Communications, 13(4), pp. 56–61, 2006. https://doi.org/10.1109/MWC.2006.1678166

[5] Ghorbani, M., Sharifzadeh, M. "Long term stability assessment of Siah Bisheh powerhouse cavern based on displacement back analysis method", Tunnelling and Underground Space Technology, 24(5), pp. 574–583, 2009. https://doi.org/10.1016/j.tust.2009.02.007

[6] Cepuritis, P. M. "The use of scale independent shape measures to assess open stope performance", International Journal of Rock Mechanics and Mining Sciences, 48(7), pp. 1188–1195, 2011. https://doi.org/10.1016/j.ijrmms.2011.07.005

[7] Hamrouni, A., Dias, D., Sbartai, B. "Reliability analysis of a mechanically stabilized earth wall using the surface response methodology optimized by a genetic algorithm", Geomechanics and Engineering, 15(4), pp. 937–945, 2018. https://doi.org/10.12989/gae.2018.15.4.937

[8] Lafifi, B., Rouaiguia, A. "Investigation of reliability analysis of shallow foundation by combining Hasofer-Lind index, response surface methodology and multi-objective genetic algorithm", International Journal of Reliability and Safety, 15(1–2), pp. 18–36, 2021. https://doi.org/10.1504/IJRS.2021.10043286

[9] Sasmal, S. K., Behera, R. N. "Prediction of combined static and cyclic load-induced settlement of shallow strip footing on granular soil using artificial neural network", International Journal of Geotechnical Engineering, 15(7), pp. 834–844, 2018. https://doi.org/10.1080/19386362.2018.1557384

[10] Khan, S. Z., Suman, S., Pavani, M., Das, S. K. "Prediction of the residual strength of clay using functional networks", Geoscience Frontiers, 7(1), pp. 67–74, 2016. https://doi.org/10.1016/j.gsf.2014.12.008

[11] Jahed Armaghani, D., Shoib, R. S. N. S. B. R., Faizi, K., Rashid, A. S. A. "Developing a hybrid PSO–ANN model for estimating the ultimate bearing capacity of rock-socketed piles", Neural Computing and Applications, 28(2), pp. 391–405, 2017. https://doi.org/10.1007/s00521-015-2072-z

[12] Cheng, J., Li, Q. S., Xiao, R. "A new artificial neural network-based response surface method for structural reliability analysis", Probabilistic Engineering Mechanics, 23(1), pp. 51–63, 2008. https://doi.org/10.1016/j.probengmech.2007.10.003

[13] Shu, S., Gong, W. "An artificial neural network-based response surface method for reliability analyses of c-φ slopes with spatially variable soil", China Ocean Engineering, 30(1), pp. 113–122, 2016. https://doi.org/10.1007/s13344-016-0006-x

[14] Haeri, S. M., Khosravi, A., Garakani, A. A., Ghazizadeh, S. "Effect of Soil Structure and Disturbance on Hydromechanical Behavior of Collapsible Loessial Soils", International Journal of Geomechanics, 17(1), 04016021, 2017. https://doi.org/10.1061/(ASCE)GM.1943-5622.0000656

[15] Zhang, Y., Chen, C., Lei, P., Wang, Z., Jiao, W. "Experimental investigation on ceiling flame extension subject to relative large area of liquid fuel in a channel-like structure with confined portals", Tunnelling and Underground Space Technology, 112, 103899, 2021. https://doi.org/10.1016/j.tust.2021.103899

[16] Li, Z.-W., Yang, X.-L. "Stability assessment of 3D reinforced soil structures under steady unsaturated infiltration", Geotextiles and Geomembranes, 50(3), pp. 371–382, 2022. https://doi.org/10.1016/j.geotexmem.2021.11.005

[17] Padmini, D., Ilamparuthi, K., Sudheer, K. P. "Ultimate bearing capacity prediction of shallow foundations on cohesionless soils using neurofuzzy models", Computers and Geotechnics, 35(1), pp. 33–46, 2008. https://doi.org/10.1016/j.compgeo.2007.03.001

[18] Xue, X., Yang, X. "Application of the adaptive neuro-fuzzy inference system for prediction of soil liquefaction", Natural Hazards, 67(2), pp. 901–917, 2013. https://doi.org/10.1007/s11069-013-0615-0

[19] Harandizadeh, H., Toufigh, M. M., Toufigh, V. "Application of improved ANFIS approaches to estimate bearing capacity of piles", Soft Computing, 23(19), pp. 9537–9549, 2019. https://doi.org/10.1007/s00500-018-3517-y

[20] Bentley Systems, Inc. "Plaxis 2D (V8.6)", Finite Element Code for Soil and Rock Analysis, [computer program] Available at: http://www.plaxis.nl/ie.html

[21] Lemaire, de M. "Fiabilité des structures: Couplage mécano-fiabiliste statique" (Structural Reliability: Static Mechano-Reliability Coupling), European Journal of Computational Mechanics, 15(7–8), pp. 989–992, 2006. (in French) https://doi.org/10.1080/17797179.2006.9737269

[22] Hasofer, A. M., Lind, N. C. "Exact and Invariant Second-Moment Code Format", Journal of the Engineering Mechanics Division, 100(1), pp. 111–121, 1974. https://doi.org/10.1061/JMCEA3.0001848

[23] Sekfali, N., Belabed, L. "Reliability of geotechnical structures: case of bearing capacity failure of strip footing", Arabian Journal of Geosciences, 11(12), 296, 2018. https://doi.org/10.1007/s12517-018-3649-5

[24] Fieβler, B., Hawranek, H., Rackwitz, R. "Numerische Methoden für probabilistische Bemessungsverfahren und Sicherheitsnachweise" (Numerical Methods for Probabilistic Design Procedures and Safety Verification), Sonderforschungsbereich 96, Laboratorium für den konstruktiven Ingenieurbau (LKI), Technische Universität München, München, Germany, 1976. (in German)

[25] Rosenblatt, M. "Remarks on a Multivariate Transformation", The Annals of Mathematical Statistics, 23(3), pp. 470–472, 1952. https://doi.org/10.1214/aoms/1177729394

[26] Chen, X., Lind, N. C. "Fast Probability Integration by Three-Parameter Normal Tail Approximation", Structural Safety, 1(4), pp. 269–276, 1983. https://doi.org/10.1016/0167-4730(82)90003-0

[27] Myers, R. H., Montgomery, D. C., Vining, G. G., Robinson, T. J. "Generalized Linear Models: With Applications in Engineering and the Sciences", John Wiley & Sons, 2010. ISBN 9780470454633 https://doi.org/10.1002/9780470556986

[28] Zerti, A., Yallese, M. A., Meddour, I. Belhadi, S., Haddad, A., Mabrouki, T. "Modeling and multi-objective optimization for minimizing surface roughness, cutting force, and power, and maximizing productivity for tempered stainless steel AISI 420 in turning operations", The International Journal of Advanced Manufacturing Technology, 102, pp. 135–157, 2019. https://doi.org/10.1007/s00170-018-2984-8

[29] Izquierdo, M., Querol, X., Davidovits, J., Antenucci, D., Nugteren, H., Fernández-Pereira, C. "Coal fly ash-slag-based geopolymers: Microstructure and metal leaching", Journal of Hazardous Materials, 166(1), pp. 561–566, 2009. https://doi.org/10.1016/j.jhazmat.2008.11.063

[30] Calise, F., Macaluso, A., Pelella, L., Vanoli, L. "A comparison of heat transfer correlations applied to an Organic Rankine Cycle", Engineering Science and Technology, an International Journal, 21(6), pp. 1164–1180, 2018. https://doi.org/10.1016/j.jestch.2018.09.009

[31] Tanyildizi, H. "Long-term performance of the healed mortar with polymer containing phosphazene after exposed to sulfate attack", Construction and Building Materials, 167, pp. 473–481, 2018. https://doi.org/10.1016/j.conbuildmat.2018.02.054

[32] Kim, M., Hizir, O., Turan, O., Day, S., Incecik, A. "Estimation of added resistance and ship speed loss in a seaway", Ocean Engineering, 141, pp. 465–476, 2017. https://doi.org/10.1016/j.oceaneng.2017.06.051

[33] Meddour, I., Messekher, S. E., Younes, R., Yallese, M. A. "Selection of bearing health indicator by GRA for ANFIS-based forecasting of remaining useful life", Journal of the Brazilian Society of Mechanical Sciences and Engineering, 43(3), 144, 2021. https://doi.org/10.1007/s40430-021-02878-w

[34] Alarifi, I. M., Nguyen, H. M., Naderi Bakhtiyari, A., Asad, A. "Feasibility of ANFIS-PSO and ANFIS-GA models in predicting thermophysical properties of Al_2O_3-MWCNT/oil hybrid nanofluid", Materials, 12(21), 3628, 2019. https://doi.org/10.3390/ma12213628

[35] Ren, J., Toniolo, S. "Life cycle sustainability decision-support framework for ranking of hydrogen production pathways under uncertainties: An interval multi-criteria decision making approach", Journal of Cleaner Production, 175, pp. 222–236, 2018. https://doi.org/10.1016/j.jclepro.2017.12.070

[36] Flavigny, E., Desrues, J., Palayer, B. "Note Technique: Le Sable d'Hostun «RF»" (Technical Note: Hostun «RF» Sand), Revue Française de Géotechnique, 53, pp. 67–70, 1990. (in French) https://doi.org/10.1051/geotech/1990053067

[37] Abdelouhab, A., Dias, D. Freitag, N. "Numerical analysis of the behavior of mechanically stabilized earth walls reinforced with different types of strips", Geotextiles and Geomembranes, 29(2), pp. 116–129, 2011. https://doi.org/10.1016/j.geotexmem.2010.10.011

[38] Montgomery, D. C. "Design and analysis of experiments", John Wiley & Sons, 2001. ISBN 9780471316497

[39] Wolff, T. H. "Analysis and design of embankment dam slopes a probabilistic approach (soil mechanics, Indiana)", PhD Dissertation, Purdue University, 1985.

[40] Griffiths, D. V., Huang, J., Fenton, G. A. "Probabilistic infinite slope analysis", Computers and Geotechnics, 38(4), pp. 577–584, 2011. https://doi.org/10.1016/j.compgeo.2011.03.006

[41] Sivakumar Babu, G. L., Srivastava, A. "Reliability analysis of allowable pressure on shallow foundation using response surface method", Computers and Geotechnics, 34(3), pp. 187–194, 2007. https://doi.org/10.1016/j.compgeo.2006.11.002

[42] Youssef Abdel Massih, D. S., Soubra, A.-H. "Reliability-based analysis of strip footings using response surface methodology", International Journal of Geomechanics, 8(2), pp. 134–143, 2008. https://doi.org/10.1061/(ASCE)1532-3641(2008)8:2(134)

[43] Myers, R. H., Montgomery, D. C., Anderson-Cook, C. M. "Response surface methodology: process and product optimization using designed experiments", John Wiley & Sons, 2016. ISBN 978-1-118-91601-8

[44] State-Ease, Inc. "Design Expert (V10)", Statistical Software Package, [computer program] Available at: https://www.statease.com/software/design-expert/

[45] Betiku, E., Odude, V. O., Ishola, N. B., Bamimore, A., Osunleke, A. S., Okeleye, A. A. "Predictive capability evaluation of RSM, ANFIS and ANN: A case of reduction of high free fatty acid of palm kernel oil via esterification process", Energy Conversion and Management, 124, pp. 219–230, 2016. https://doi.org/10.1016/j.enconman.2016.07.030

[46] The MathWorks, Inc. "Matlab Software (R2015b)", [computer program] Available at: https://www.mathworks.com/products/matlab.html

[47] Khellaf, A., Aouici, H., Smaiah, S., Boutabba, S., Yallese, M. A., Elbah, M. "Comparative assessment of two ceramic cutting tools on surface roughness in hard turning of AISI H11 steel: including 2D and 3D surface topography", The International Journal of Advanced Manufacturing Technology, 89(1), pp. 333–354, 2017. https://doi.org/10.1007/s00170-016-9077-3

[48] Suresh Kummar Reddy, N., Venkateswara Rao, P. "Selection of optimum tool geometry and cutting conditions using a surface roughness prediction model for end milling", The International Journal of Advanced Manufacturing Technology, 26(11–12), pp. 1202–1210, 2005. https://doi.org/10.1007/s00170-004-2110-y

[49] Nottrodt, H.-P. "Beitrag zur Einfhrung semiprobabilistischer Methoden in der Geotechnik" (Contribution to the introduction of semi-probabilistic methods in geotechnics), Dissertation, Hochschule für Architektur und Bauwesen Weimar, 1990. (in German)